

# On the stability & phase locking to a system reference of an optoelectronic oscillator with large delay

This paper was downloaded from TechRxiv (<https://www.techrxiv.org>).

LICENSE

CC BY 4.0

SUBMISSION DATE / POSTED DATE

09-08-2020 / 16-08-2020

CITATION

Hasan, Mehedi (2020): On the stability & phase locking to a system reference of an optoelectronic oscillator with large delay. TechRxiv. Preprint. <https://doi.org/10.36227/techrxiv.12782531.v1>

DOI

[10.36227/techrxiv.12782531.v1](https://doi.org/10.36227/techrxiv.12782531.v1)

# On the stability & phase locking to a system reference of an optoelectronic oscillator with large delay

Mehedi Hasan<sup>1\*</sup>, Charles Nicholls<sup>2</sup>, Trevor Hall<sup>1</sup>

<sup>1</sup> Photonic Technology LAB, University of Ottawa, 25 Templeton Street, Ottawa, ON, Canada, K1N 6X1

<sup>2</sup> NANOWAVE Technologies Inc., 6 Gurdwara Rd, Nepean, ON, Canada, K2E 8A3

\*[mhasa067@uottawa.ca](mailto:mhasa067@uottawa.ca)

## Abstract

Delay line oscillators based on photonic components, offer the potential for realization of phase noise levels up to 3 orders of magnitude lower than achievable by conventional microwave sources. The quality factor of such oscillators is proportional to the delay. Fibre optic based delay lines can realize the large delay required for high quality factor low phase noise systems whilst simultaneously achieving insertion loss levels that can be compensated for with available microwave and photonic amplification technologies. Multi-mode operation is an artefact of the delay line oscillator and introduces instability into phase locked control loops as a result of the multiplicity of available locking signals. An optoelectronic oscillator (OEO) with large delay under proportional and proportional integral control by a phase-locked loop (PLL) is modelled; providing the first report of the location of all of the infinity of poles of the system function. The first experimental observations of giant phase modulation oscillation of a free OEO and spontaneous phase modulated oscillation of a PLL-OEO are also reported and explained. Nevertheless, the analysis and experimental observations, including a prototype 10 GHz PLL-OEO phase noise spectral density achieving  $-80 \text{ dBc/Hz}$  at 10 Hz and  $-145 \text{ dBc/Hz}$  at 10 kHz, demonstrate that stable phase lock operation and optimum phase noise performance is achievable provided full account of the multimode operation of the basic oscillator is taken in the phase lock analysis.

## I. Introduction

The random fluctuations of an oscillator limit the precision of time and frequency measurements on which scientific and technological endeavours rely. The noise and long-term stability of the system oscillator / clock is of major importance in applications such as optical and wireless communications, high-speed digital electronics, radar, and astronomy. With ever-increasing clock frequencies being used in digital systems the requirement for compact high performance clock sources will continue. The development of such a source would have major impact, for example, on radar sensitivity through improved clutter rejection; on the generation of mm waves for 5G wireless and research into sources of THz radiation.

Among a variety of means using photonics to generate microwaves, the optoelectronic oscillator (OEO) is the most suited to practical deployment. Reference [1] provides a review of the large literature that has arisen following the introduction in 1996 of the OEO [2]. Lasers and OEOs are examples of time delay oscillators. The laser generates optical carriers using a cavity containing the sustaining amplifier. The OEO generates microwave carriers using an RF photonic link consisting of laser; optical intensity modulator; optical fibre; photo-receiver; RF amplifier and bandpass filter, which drives the modulator; closing the loop and sustaining oscillation. The virtue of time delay oscillators is the large delay achievable relative to the oscillation period. The low loss of optical fibre (0.2 dB/km) permits delay line lengths of  $\sim 10$  km offering exceptional OEO phase noise performance. However, the frequency interval between adjacent oscillator modes becomes very small (20 kHz for 10 km), and filtering is needed for mode selection and side-mode suppression.

Whereas quartz crystal system reference oscillators, even when multiplied to microwave frequencies, offer superior phase noise at close to carrier offset frequencies, the OEO offers superior phase noise performance at offset frequencies further out from the carrier. It remains a requirement to phase lock the OEO to the system reference to reduce the close in phase noise and provide long-term stability while engineering the phase locked loop (PLL) to take advantage of the superior phase noise of a free OEO at higher offset frequencies.

A variety of architectures and approaches to locking an OEO to a system reference have been disclosed in the literature [3-8]. In most cases, the PLL is combined with injection locking; either external-injection locking of the OEO to the reference carrier [6] or self-injection locking of the OEO to a delayed replica of the oscillation [7, 8]. The latter category encompasses dual loop OEO [5] and more generally multi-loop OEOs as a large self-injection level special case. The theoretical models disclosed to describe these architectural variations, in respect of injection locking, reduce to the differential equations of Adler (weak injection) [9] or Paciorek (strong injection) [10], and, in respect of the PLL reduce to the classical model in which the voltage controlled oscillator (VCO) is treated as an integrator. It is established that injection locking has an equivalent representation as a type-I PLL [11], i.e. a proportional controller so these architectures may be viewed from the perspective of self-referenced phase locked loops which has been applied to the study of self-injection locked electronic oscillators and a short loop OEO [3]. In all cases the VCO is treated as a single mode oscillator (i.e. a phase integrator). Most often no account is taken of the delay albeit [3] accounts for the delays of the loops in the discriminator that provides the self-referencing and [5] use a second order Padé approximation to model an input delay to the integrator model of the VCO. The multimode operation and long delay is fundamental to the neuromorphic application of a broadband OEO as a reservoir computer [12, 13] but this paper is concerned with the OEO as a source of pristine RF carriers.

A single-loop OEO under proportional and proportional integral control by a PLL is modelled taking full account of the delay; providing the first report of the location of all of the infinity of poles of the system function. This provides a well characterised basic subsystem from which more complex architectures may be considered to be composed, either as nested control loops or as coupled oscillators. The theoretical considerations are supported by experimental observations. The first observation is reported of an OEO exhibiting a giant phase modulation mode related to the FM mode regime of a mode-locked laser but without the pulse mode-locked regime. The giant phase modulation is a manifestation of a modulation instability of a PLL-OEO system which is described by the analysis and observed experimentally. Nevertheless, the analysis and experimental observations presented demonstrate that stable phase lock operation and optimum phase noise performance is achievable if the presence of multimode operation of the basic oscillator is accounted for in the phase lock analysis.

This paper is organized as follows. In section II the complete system model of a PLL-OEO is formulated. In section III all the poles in the complex plane of the system function describing a free OEO are located. Section IV reports the observation of giant phase modulation of an OEO oscillation is reported and explained theoretically. Section V reports the observation of spontaneous phase oscillation of a PLL-OEO. Section VI describes the location of all the poles of a PLL-OEO system under proportionate and proportional integral control laying the ground for a description of the origins of the weak modulation instability in Section VII on the active loop filter. Section VIII reports the experimental demonstration of a stable PLL-OEO with near optimal phase noise spectral density. Finally, Section IX concludes the paper with a summary and discussion of the main findings.

## II. System analysis

The behaviour of a phase locked loop (PLL) is accurately captured by a dynamical system model with the phase of the voltage controlled oscillator as state variable. An orthodox voltage-controlled oscillator (VCO) is modelled as a perfect integrator characterized by its tuning sensitivity  $K_{VCO}$  ( $Hz/V$ ). The phase sensitive detector (PSD) may be based on a balanced mixer or other approximation to a four-quadrant multiplier, which provides an approximately sinusoidal response with  $2\pi$  period. An alternative implementation based on sequential phase detector combined with a charge pump provides a linear response over an interval of  $(-2\pi, 2\pi)$  outside of which the response saturates. In either case, the PSD is characterised by its sensitivity  $K_{VCO}$  ( $V/rad$ ) to small phase differences. The loop filter is modelled by a linear system of differential equations which is expressed equivalently but more conveniently by the system function in the Laplace transform domain. Indeed subject to linearization, the closed loop system function of the complete PLL may be derived and its poles (and zeros) located. Since the number of poles is small, it is a relatively simple

design matter to place all the poles in the left-hand half-plane of the Laplace transform domain to ensure stability.

An optoelectronic oscillator (OEO) may be tuned by inserting a voltage controlled phase shifter within the oscillating path (see Figure 4). The path contains an optical fibre coil of substantial length ( $\sim 5\text{km}$ ) and hence long delay ( $\sim 25\ \mu\text{s}$ ). The OEO oscillation essentially accumulates a phase shift step on each round trip which results in a staircase approximation of the linear ramp in oscillator phase provided by an orthodox VCO. The difference between the staircase and the ramp is a sawtooth with period equal to the round trip time. The Fourier series of this sawtooth reveals the excitation of adjacent side-modes of the main oscillation mode by the initial step. The staircase step is smoothed on each round trip and the side-modes progressively suppressed by the RF bandpass filter placed within the loop precisely to promote single mode oscillation. However, the passband of the RF filter is large ( $\sim 3\ \text{MHz}$ ) compared to the frequency interval between adjacent side-mode modes ( $\sim 40\ \text{kHz}$ ) and many hundreds of round trips are necessary before the smoothing is effective. The OEO is an example of a time delay oscillator and its behaviour as a voltage controlled oscillator differs substantially from an orthodox VCO.

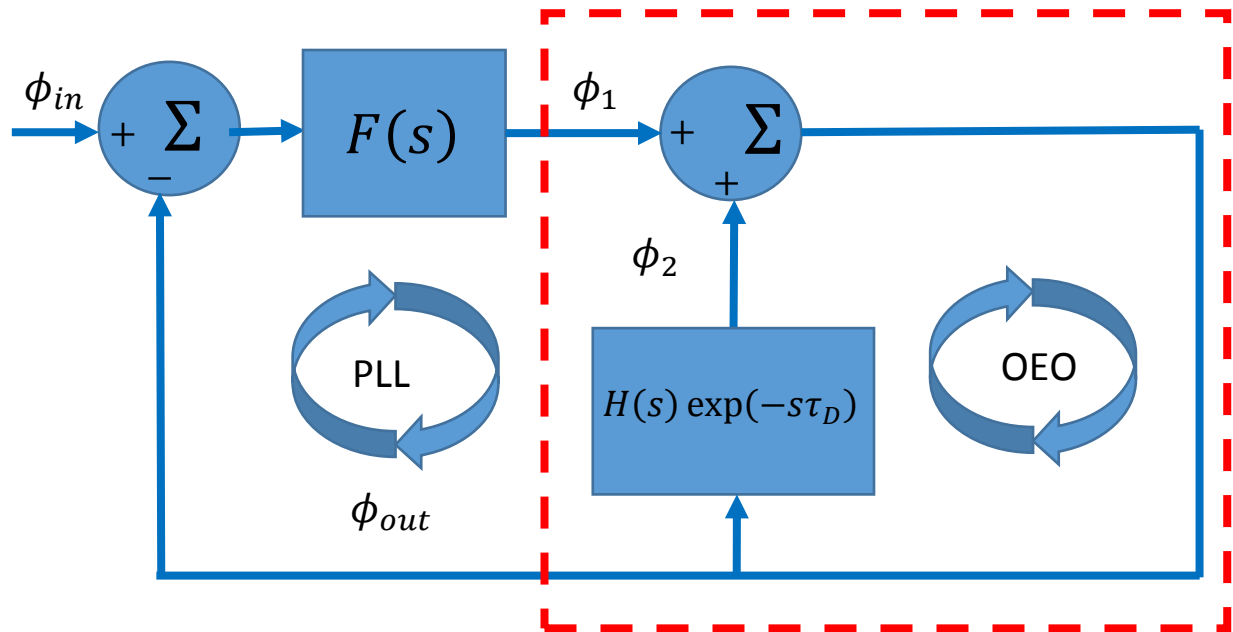


Figure 1 Phase model of a phase locked optoelectronic oscillator system. The phase locked loop form a negative feedback loop composed of the phase sensitive detector (PSD), loop filter, and optoelectronic oscillator (OEO). The PSD is depicted by the signed summation block on the left that measures the phase error  $\phi_{in} - \phi_{out}$ . The loop filter is depicted by a block labelled by its system function  $F$ . The OEO is depicted by the contents the dashed box that form a positive feedback loop. The rectangle represents the action of the time delay  $\tau_D$  and the RF filter in the Laplace transform domain.  $H$  is the baseband equivalent system function of the RF bandpass filter. The summation block represents a phase shifter that introduces a single pass phase shift equal to the tuning control  $\phi_1$

Systems with time delays such an OEO are challenging to control [14]. Their stability analysis is complicated by a system function possessing an infinite number of poles. In practice, one can only locate a finite number of these poles and consequently, while a controller may be designed to place the finite number known poles in the left-hand half-plane of the Laplace transform domain, one rarely can be certain that the same controller has not shifted one or more of the remaining infinity of poles into the right-hand half-plane, thereby leading to instability. However, with careful analysis of a PLL-OEO system, stable phase lock in the presence of an infinite number of poles has been demonstrated to be achievable.

With the aid of the Leeson model of the oscillator [15], the complete system is modelled as a linear time invariant system with phase as state variable. The oscillation frequency is varied by an adjustable phase shifter within the oscillating path. It is convenient to take the signal input to the phase sensitive detector from the output coupler of the oscillator, which leads to the configuration illustrated schematically by Figure 1. The multiscale analysis method applied herein takes advantage of three distinct timescales:

$$\tau_F \gg \tau_D \gg \tau_R$$

*Equation 1*

where the time constants  $\tau_F, \tau_D, \tau_R$  are characteristic of the loop filter; the oscillator time delay; and the RF bandpass filter. The ordering of the parameters is consistent with practical application where the orders of magnitude are  $\tau_F \sim \mathcal{O}(10^2)$ ,  $\tau_D \sim \mathcal{O}(10^0)$ ,  $\tau_R \sim \mathcal{O}(10^{-2})$ .

The complete system function is:

$$K = \frac{FG}{1 + FG}$$

*Equation 2*

where  $F$  is the loop filter system function; and  $G$  is the system function of a Leeson model of a time-delay oscillator given by:

$$G(s) = \frac{1}{1 - H(s) \exp(-\tau_D s)}$$

*Equation 3*

where  $\tau_D$  is the delay and  $H$  is the baseband equivalent transfer function of a bandpass filter that promotes single-mode oscillation; a single-pole model characterised by the time constant  $\tau_R$  is used for simplicity:

$$H(s) = \frac{1}{1 + \tau_R s}$$

*Equation 4*

Substitution of Equation 4 and Equation 3 into Equation 2 gives the overall system function of the phase-locked loop:

$$K(s) = \frac{F(s)}{1 + F(s) - \frac{1}{1 + \tau_R s} \exp(-\tau_D s)}$$

*Equation 5*

### III. Free optoelectronic oscillator system pole location

Initially consider the controlled optoelectronic oscillator shown within the red dashed box in Fig. 1. Substituting Equation 4 into Equation 3 gives free-oscillator system function:

$$G(s) = \frac{1}{1 - \frac{1}{1 + s\tau_R} \exp(-s\tau_D)}$$

*Equation 6*

The poles are located at the roots of the characteristic equation:

$$\chi(s) = 1 + s\tau_R - \exp(-s\tau_D)$$

*Equation 7*

The equation for the roots  $\chi(s) = 0$  may be recast into an equation:

$$(\rho + \tau_D s) \exp(\rho + \tau_D s) = \rho \exp(\rho) \quad ; \quad \rho = \tau_D / \tau_R$$

*Equation 8*

that has same form as the definition of the Lambert  $w$  function<sup>1</sup> [16]:

$$w(z) \exp(w(z)) = z$$

Equation 9

Hence:

$$s_k \tau_D = w_k(\rho \exp(\rho)) - \rho \quad ; \quad k \in \mathbb{Z}$$

Equation 10

where the integer  $k$  indexes the countable infinity of branches of the multivalued Lambert  $w$  function. The Lambert  $w$  function organises its solutions by increasing negative real part with increasing magnitude of the branch index. It is therefore only necessary to examine the  $k = 0$  branch to determine the stability of the system.

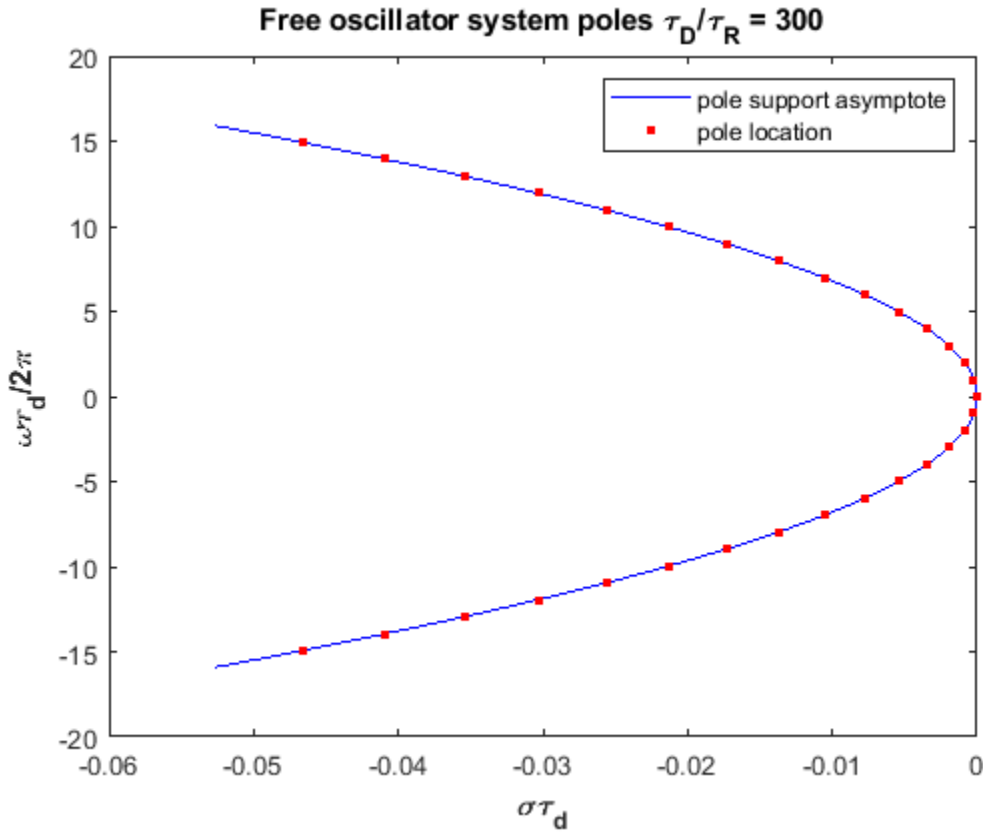


Figure 2 A comparison of the predicted location of the poles of the characteristic function of a free time delay oscillator and the asymptotic curve defined by Equation 13

Expressed in terms of the real  $\sigma$  and imaginary  $i\omega$  parts of the Laplace transform variable  $s$  the equation  $\chi(s) = 0$  separates into two coupled real equations:

$$\tau_D \sigma = -\frac{1}{2} \ln((1 + \tau_D \sigma / \rho)^2 + (\tau_D \omega / \rho)^2)$$

Equation 11

$$\tau_D \omega = 2\pi k - \tan^{-1}(\tau_R \omega / (1 + \tau_R \sigma)) \quad ; \quad k \in \mathbb{Z}$$

Equation 12

Equation 11 implicitly defines a continuous curve parameterised by  $\tau_R \omega$  on which the poles must lie in the complex plane and Equation 12 implicitly discretizes the curve into a countably infinity of samples at which

<sup>1</sup> The Lambert  $w$  function is a Matlab supplied function.

the poles are located. These equations define a contractive mapping which may be iterated as an alternative to the evaluation of the Lambert  $w$  function.

For  $\rho \gg 1$  the poles approach an explicitly defined curve:

$$\tau_D \sigma(\tau_R \omega) = -\frac{1}{2} \ln(1 + (\tau_R \omega)^2)$$

*Equation 13*

which provides an excellent fit to the distribution of the poles for practical values of the  $\rho$  parameter (see Figure 2) and provides an upper bound to their real part. Such curves are of great utility in establishing necessary conditions for stability of controlled time delay oscillator systems without explicit solution in terms of elementary or special functions [17].

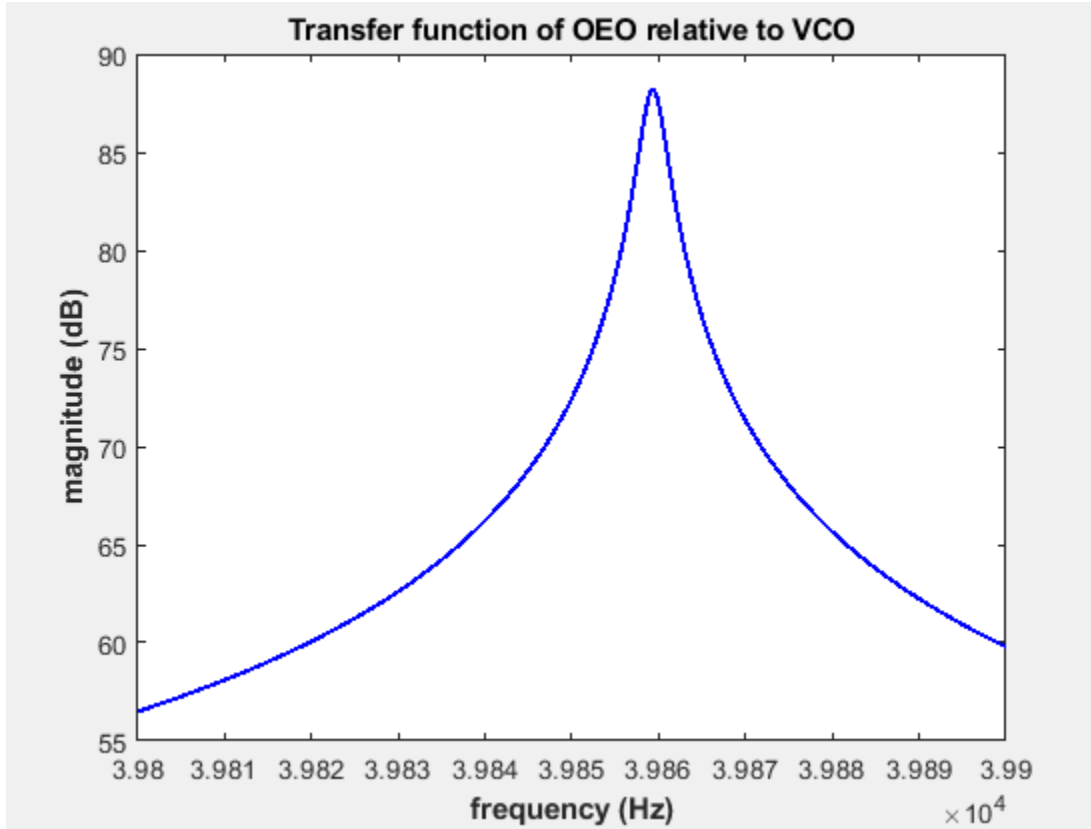


*Figure 3 Simulated transfer function of an optoelectronic voltage controlled oscillator relative to an orthodox voltage-controlled oscillator with equivalent static gain-in a neighbourhood of the first resonance.*

#### IV. Giant phase modulation

The controlled optoelectronic oscillator shares with an orthodox voltage-controlled oscillator a pole at the origin representing a perfect integrator; it also exhibits an additional countable infinity of complex conjugate pairs of poles in the left-hand half-plane close to the imaginary axis representing resonances at frequencies  $\omega_m$  close to multiples of the reciprocal of the loop delay:

$$\omega_m \tau_D = 2k\pi \quad k \in \mathbb{Z}$$

*Equation 14*

A single-pass intra-loop phase shift that is modulated is amplified by a modulation-frequency-dependent gain  $G$  given for an OEO by *Equation 6* and for an orthodox VCO with equivalent quasi-static tuning sensitivity by:

$$G(s) \rightarrow 1/s\tau_D \quad ; \quad s \rightarrow 0$$

Equation 15

Consequently, the system function  $R(s)$  of the controlled optoelectronic oscillator *relative* to an orthodox voltage-controlled oscillator is given by:

$$R(s) = \frac{s\tau_D}{1 - (1/(1 + s\tau_R)) \exp(-s\tau_D)}$$

Equation 16

The precise resonant frequency is slightly detuned by the phase contributed by the RF-bandpass filter from the value predicted by Equation 14. Substitution of Equation 14 with a small detuning into Equation 16 and adjusting the detuning to obtain a real denominator provides an estimate of the magnitude of the resonant peaks:

$$R \rightarrow \frac{1}{\pi} \left( \frac{\tau_D}{\tau_R} \right)^2 \frac{1}{k^2} = 28650 \text{ (89 dB)} \quad k = 1$$

Equation 17

This value is confirmed by a plot of the relative transfer function shown in Figure 3 which shows the first resonance reaching 89 dB in relative magnitude. Before neglecting resonances of such magnitude one must be confident that nevertheless their impact on system behaviour is insignificant.

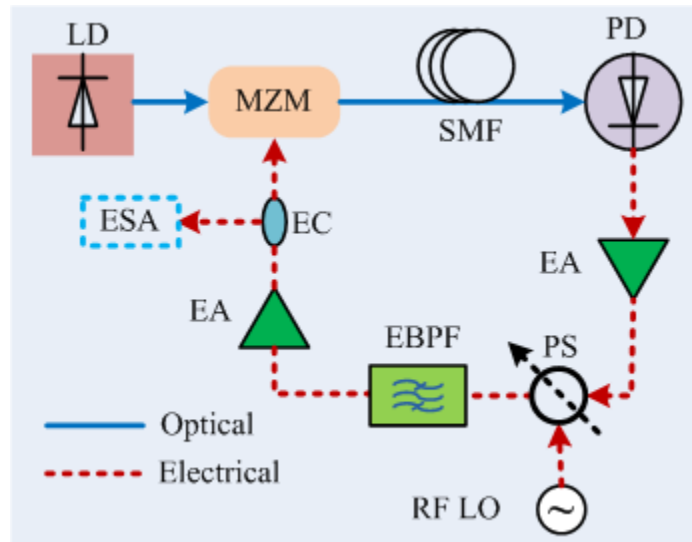


Figure 4 Schematic diagram of the proposed experimental setup. LD, Laser diode; MZM, Mach-Zehnder modulator; SMF, Single mode fiber; PD, Photodiode; EA, Electrical amplifier; PS, Phase shifter; EBPF, Electrical bandpass filter; EC, Electrical coupler; ESA, Electrical spectrum analyzer; RF LO, Radio frequency local oscillator.

To confirm these resonances experimentally, a small voltage modulation is applied to a voltage controlled RF phase shifter inserted within the OEO loop. The experimental arrangement is shown schematically in Figure 4. A resonator made for another application having quality factor of around  $\sim 2700$  is used as the electrical bandpass filter (EBPF). A distributed feedback (DFB) laser having an output power of 80 mW with an operating wavelength near  $\sim 1550.12$  nm is used as the optical source. The Analog Devices HMC931 phase shifter (PS) is used in the demonstration. The electrical amplifiers are off-the-shelf power amplifiers having a gain of 16 dB. Three similar electrical amplifiers were used in the loop to compensate the extra insertion losses caused by EBPF ( $\sim 10$  dB) and PS ( $\sim 4$  dB).

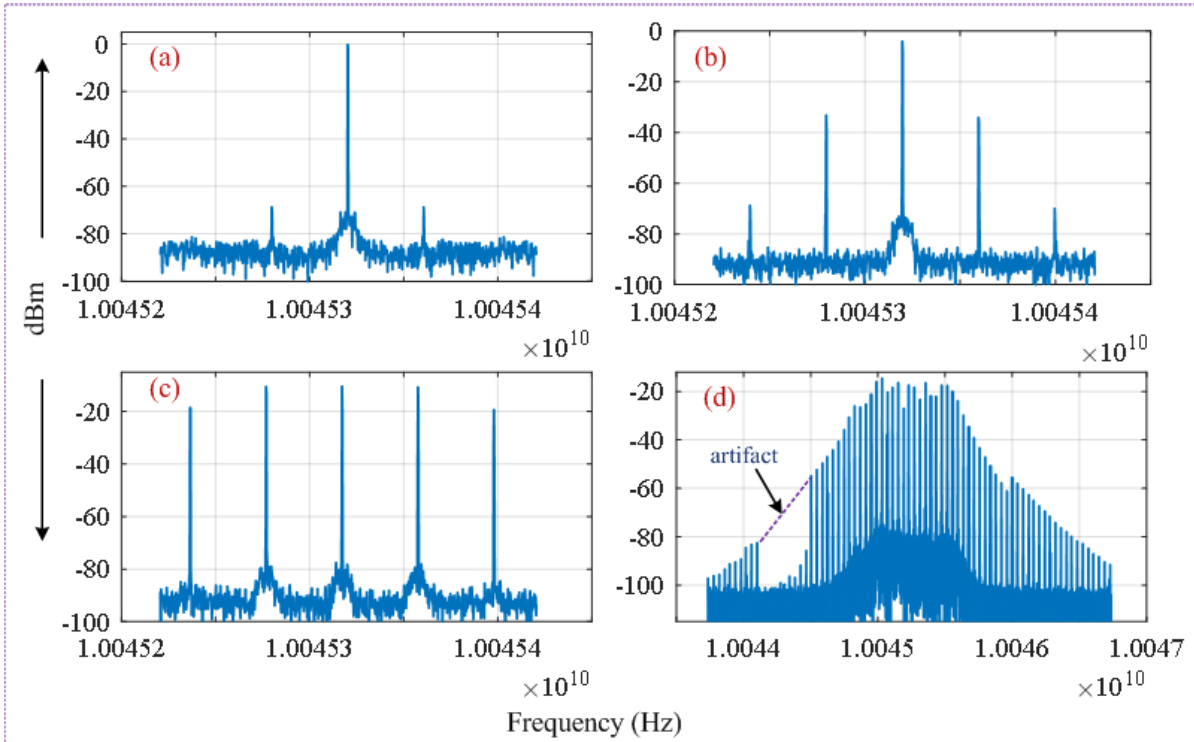


Figure 5 Measured electrical spectrum for (a) free run OEO and; (b-d) with small injection of sinusoid close to the mode spacing. A resolution bandwidth of 100 Hz is used for all the measurement. A span of 200 kHz is used for (a-c); whereas a span of 3 MHz is used for (d).

Figure 5 (a) shows the measured electrical spectrum of the OEO without any applied modulation. The spurs are separated from the oscillation frequency by the inverse of delay produced by a 5 km optical fibre coil. A sinusoidal voltage with 40 kHz frequency and -50 dBm power is applied to the phase shifter (PS) to introduce intra-loop phase modulation. Figure 5(b) shows the resulting measured electrical spectrum of the RF output of the OEO. It shows that with modulation the side modes (spurs) gain considerable power in comparison to the spectrum without any injected phase modulation (Figure 5(a)). At modulation frequencies close to resonance ( $\sim 40.38$  kHz), the outcome is giant phase modulation of the carrier confirming the prediction of *Equation 17*. The giant phase modulation generates a large number of side modes at harmonics of the modulation frequency of similar magnitude (Figure 5(c)) extending over a broad band (Figure 5(d)) comparable to the  $-3$  dB bandwidth of the electrical bandpass filter.

## V. Spontaneous phase oscillation

When locking an optoelectronic oscillator to a system frequency reference, the optoelectronic oscillator is substituted for the voltage-controlled oscillator of a phase-locked loop. The traditional approach to the design of a phase-locked loop accounts for the action of a voltage-controlled oscillator as an integrator; a constant voltage results in a change of frequency corresponding to a constant rate of change of phase. The pole at the origin of the system function described by *Equation 6* accounts for the same behaviour of an optoelectronic oscillator equipped with a voltage controlled intra-loop phase-shifter; a constant applied voltage induces a constant single-pass phase shift that is continuously accumulated each round-trip, yielding a change in oscillator frequency. However, the near singular resonances in the modulation transfer function of the optoelectronic oscillator are a source of instability and spontaneous phase-modulated oscillation may be observed on closing the phase locked loop (see Section VII).

To understand the system as a phase oscillator requires a model of the gain saturation process. In the case of a type-II PLL, the sequential phase detector and charge pump combination has a linear phase error range

of  $(-2\pi, 2\pi)$ . Beyond this range its output saturates to an upper or lower limit which results in the output of the active loop filter loop increasing or decreasing until it in turn saturates to pull the oscillation frequency of the voltage-controlled oscillator in the correct direction over the acquisition range until phase lock. The voltage controlled phase-shift  $\phi_1$  is also limited to a finite interval but a range exceeding  $(-\pi, \pi)$  provides sufficient tuning to capture adjacent RF oscillation modes but ensures that the phase-sensitive detector is the saturation mechanism.

In the case of co-sinusoidal modulation with  $\Delta\phi$  peak single-pass phase amplitude

$$\phi_1(t) = \Delta\phi \cos(\omega_m t)$$

*Equation 18*

under conditions where all significant sidebands of the oscillation fall well within the passband of the RF-bandpass filter, the Leeson model predicts a phase modulated oscillation known as a Bessel super-mode with envelope given by:

$$u(t) = \exp[i(\omega_0 t + \mu \cos(\omega_m t + \xi))] = \exp(i\omega_0 t) \sum_{n=-\infty, \infty} J_n(\mu) \exp(in(\omega_m t + \xi))$$

*Equation 19*

where  $\mu = |G(i\omega_m)|\Delta\phi$  is the magnitude and  $\xi$  the phase of the excursion of the oscillation phase,  $\Delta\phi$  is the peak intra-loop phase modulation and the expression on the right-hand side follows from the Jacobi-Anger expansion.

A more sophisticated Floquet analysis of the dynamical system describing the full complex amplitude of a laser with intra-cavity phase modulation [18] predicts a solution identical to *Equation 19* except at near zero detuning where a pulsed mode-locked solution emerges. Close to zero detuning the peak phase excursion of the phase modulated oscillation can become so great that the sidebands of the Bessel super mode reach the edge of the RF-selection filter passband which results in dissipation of their energy. The gain control mechanism of the oscillator responds by increasing the gain. The gain is homogenous so sidebands close to the carrier thereby see more gain than loss and the sidebands further away from the carrier see more loss than gain. This imbalance is sustained by the nearest-neighbour self-injection by the sidebands generated by the intra-loop phase modulation that couples the modes together providing a mechanism for the diffusion of power from the inner most sidebands to the outermost sidebands. Under these conditions a laser, which is another example of a time-delay oscillator, enters a the pulsed mode-locked oscillation regime generating a pulse train envelop with a repetition interval equal to the cavity round trip-time and with width of the order of the reciprocal of the gain bandwidth. However, in the case of a laser the saturation mechanism is the depletion of an energy reservoir: a narrow width pulse can benefit from the full energy stored in the reservoir over a round trip time. In the case of an OEO, the saturation mechanism is fast amplitude clipping: the energy available for a pulse therefore decreases as the pulse width narrows. The difference between the gain saturation mechanisms may explain why pulsed mode-locking of the OEO has not been observed in the experiments.

These observations demonstrate that the multitude of oscillation modes of an OEO render phase-locking to a system reference susceptible to instability. Hence, careful design of the loop filter is required to avoid instability while maintaining enough design freedom to achieve other goals such as robust locking dynamics and low phase-noise.

## VI. Proportional integral control

The system function described by *Equation 5* has poles located at the roots of the characteristic function:

$$\chi(s) = \tau_I s(1 + \tau_R s)(1 + F(s)) - \tau_D s \exp(-\tau_D s)$$

*Equation 20*

Simple proportional control corresponds to setting  $F = \kappa$ . Following the method of section III, the Lambert equation for the roots is then:

$$(\rho + \tau_D s) \exp(\rho + \tau_D s) = \rho \exp(\rho) / (1 + \kappa) \quad \text{Equation 21}$$

which implies:

$$s_k \tau_D = w_k (\rho \exp(\rho - \log(1 + \kappa))) - \rho \quad \text{Equation 22}$$

Equation 22 demonstrates that for  $\rho \gg |\log(1 + \kappa)|$  the proportional control displaces the poles further into the left half-plane substantially by the same amount  $\sim -\kappa$  for small proportional gain  $|\kappa| \ll 1$  (see

Figure 6).

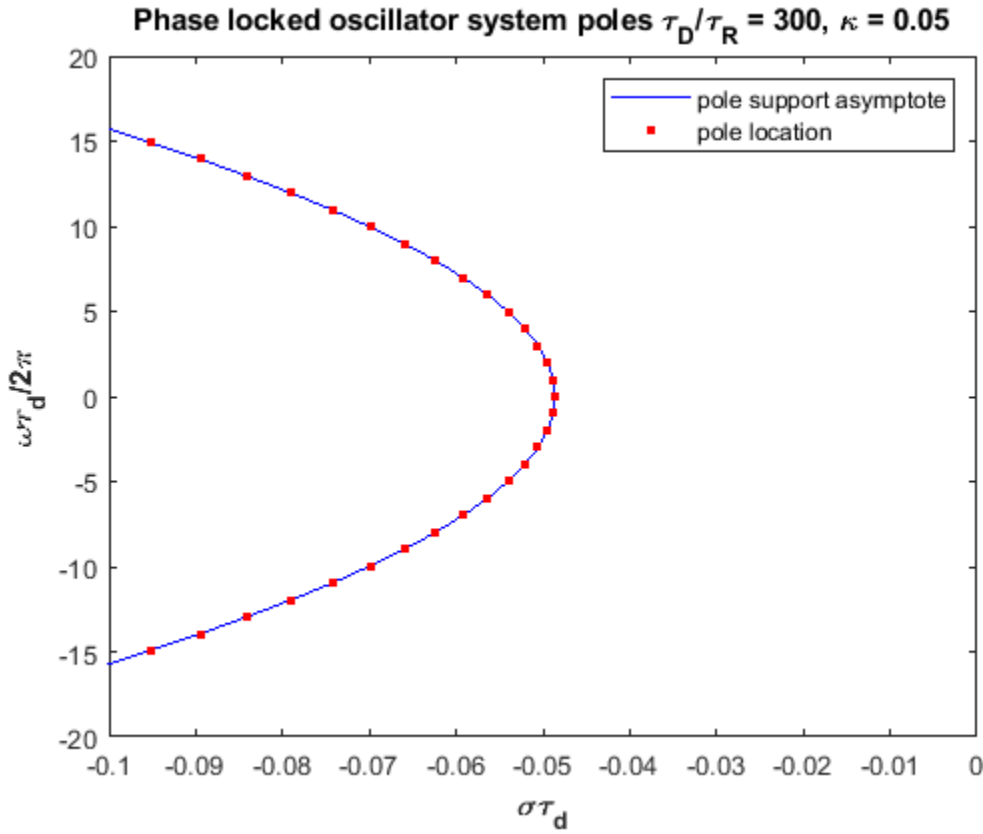


Figure 6. The predicted location of the poles of the characteristic function of a proportionally controlled time delay oscillator in the phased locked loop configuration. All poles have been displaced further along the negative real axis substantially by the proportional gain. The injection locked configuration is not shown as it is substantially the same at low gains.

Proportional control may be provided by a physical PLL or by injection locking. The damping provided by proportional control is highly effective in suppressing all the free-oscillator resonances. The oscillator oscillates but its phase is rigidly locked to the reference carrier. However, the rigidity is disadvantageous. In the case of an external system reference, the phase noise of the reference typically exceeds the phase noise of the free optoelectronic oscillator at all but the closest offset frequencies. In the case of self-referenced phase locking or self-injection locking, the phase noise of the multi-loop oscillator is degraded at best to a single loop OEO with a fibre length equal to the arithmetic average of the multiple loops.

To provide desirable system properties, such as extended lock-in range, zero steady-state error, and reduction of phase noise and suppression of spurious resonances, the characteristic function at the longest time scale should approach the quadratic equation:

$$\chi(s) \rightarrow (\tau_F s)^2 + 2\xi(\tau_F s) + 1 \quad ; \quad s\tau_F \sim \mathcal{O}(1) \quad \text{Equation 23}$$

which describes a simple harmonic oscillator with a damping factor  $\xi$  and a natural frequency  $\omega_0$  defined by:

$$\omega_0 \tau_F = 1 \quad \text{Equation 24}$$

Since:

$$\chi(s) \rightarrow \tau_I s F(s) + \tau_I \tau_D s^2 \quad ; \quad s\tau_F \sim \mathcal{O}(1) \quad \text{Equation 25}$$

it follows that:

$$F(s) \rightarrow \kappa + \frac{1}{\tau_I s} \quad ; \quad s\tau_F \sim \mathcal{O}(1) \quad \tau_F = \sqrt{\tau_I \tau_D} \quad \xi = (1/2)\kappa\sqrt{\tau_I / \tau_D} \quad \text{Equation 26}$$

which corresponds to the transfer function of a proportional integral controller. The system reference offers lower phase noise than the free oscillator only at offset frequencies below a cross-over frequency above which the free oscillator offers lower phase noise. It is therefore desirable choose the natural frequency so that roll-off of the transfer function has commenced by the crossover frequency.

There are two system poles near or on the real axis at locations close to the roots of *Equation 23*:

$$\tau_F s = -\xi \pm \sqrt{\xi^2 - 1} \quad \text{Equation 27}$$

Underdamping corresponds to  $\xi < 1$  and a complex conjugate pair of pole locations. Overdamping corresponds to  $\xi > 1$  and two real poles on the negative real axis. Excellent transient performance is offered by  $\xi = 1/\sqrt{2}$ . The remaining poles are close to the locations predicted for proportional control by *Equation 22* for all  $k \neq 0$ .

## VII. Active loop filter

The placement of the inner poles near the origin necessary for the stability of the phase locked loop established in the preceding section is not a sufficient condition for stability. The method relies on the other poles remaining close to their free-oscillator location. However, if the bandpass filter is neglected, the poles of the free-oscillator all lie on the imaginary axis. In the presence of the bandpass filter all these poles except the pole at the origin enter the left half-plane. However, the displacement of the poles representing oscillation modes that fall within the passband of the bandpass filter is slight. The introduction into the characteristic equation of the loop-filter transfer function of higher order than two is desirable for the purpose of phase noise spectrum optimisation. The resulting perturbation to the outer poles may be weak but it can be sufficient to displace poles close to the imaginary axis into the right half-plane resulting in a weakly unstable system.

The locations of the poles of the system transfer function defined by *Equation 5* satisfy:

$$\tau_D \sigma = -\ln(|Q(s)|) \quad \text{Equation 28}$$

$$\tau_D \omega = 2k\pi - \arg(Q(s)) \quad \text{Equation 29}$$

where:

$$Q = (1 + F)/H \quad \text{Equation 30}$$

Applying the ansatz:

$$|\sigma(\omega)| \ll |\omega| \Rightarrow F(s) \rightarrow \kappa ; |\tau_D \omega| \geq \mathcal{O}(1)$$

Equation 31

yields:

$$\tau_D \sigma \rightarrow -(1/2) \ln(1 + \kappa) - (1/2) \ln((1 + \tau_R \sigma)^2 + (\tau_R \omega)^2)$$

Equation 32

For large delay  $\tau_D \gg \tau_R$  the outer system poles approach the asymptotic curve that describes a proportionally controlled oscillator:

$$\tau_D \sigma(\tau_R \omega) = -(1/2) \log(1 + \kappa) - (1/2) \log(1 + (\tau_R \omega)^2)$$

Equation 33

The asymptote provides an upper bound to the distribution of the outer poles and is an excellent fit to the distribution of the poles for practical values of the parameters. The curve is entirely confined within the left half-plane, which is sufficient condition for stability provided the inner poles are similarly confined.

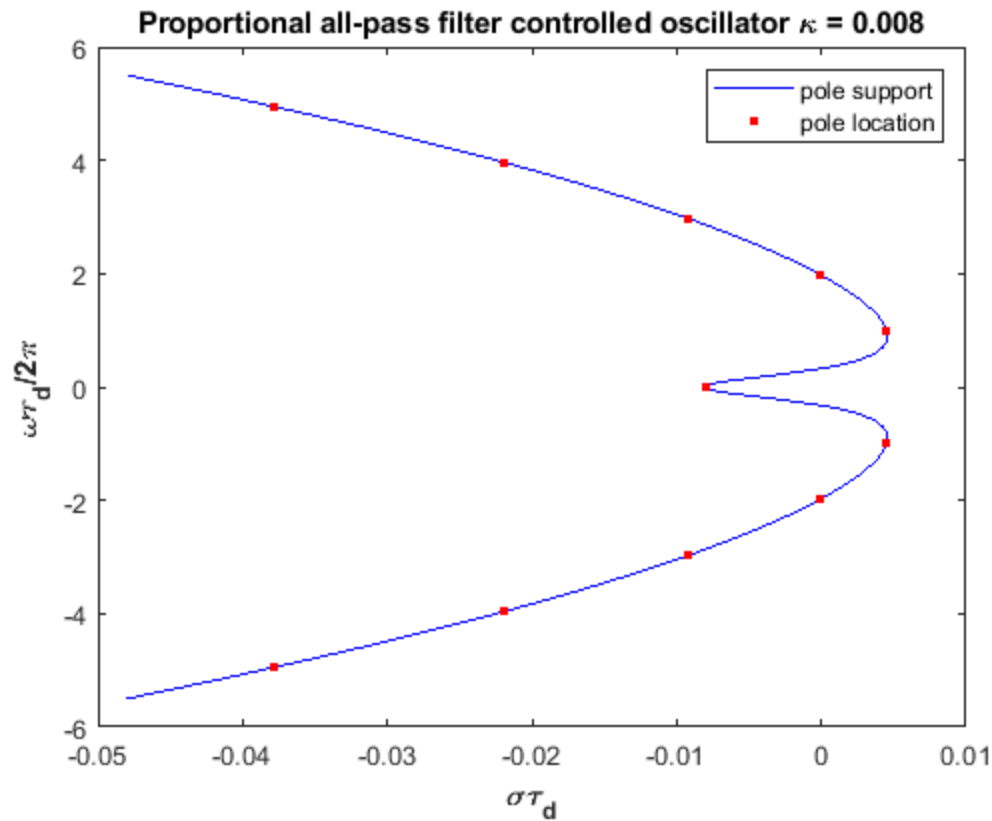


Figure 7 Displacement of the poles responsible for modulational instability. A single term all pass filter with a half-delay time constant is used as the loop-filter.

In the example given, it is significant that  $\arg(F) \rightarrow 0$  outside the neighbourhood of the origin. The phase of  $F$  plays a crucial role in Equation 28 via the term:

$$\log(|Q|^2) = \log(1 + |F|^2 + 2|F| \cos(\arg(F))) - \log(|H|^2)$$

Equation 34

Stability is only guaranteed if the cosine is positive. In practice additional poles are inserted into the transfer function of the loop filter for a variety of reasons not least of which is shaping of the phase-noise spectral density. The system reference has lower phase noise than the free oscillator in a range of low offset frequencies. It is therefore desirable that the loop filter rolls-off rapidly at higher frequencies where free-

oscillator provides superior performance. A single pole low-pass filter operating above its passband contributes a -20 dB/decade magnitude roll-off and a phase lag approaching  $-\pi/2$ . The loop filter in the prototype phase-locked OEO investigated in this study introduces three such additional poles so outside the neighbourhood of the origin the cosine term approaches  $-1$  albeit accompanied by a much reduced value of  $|F|$ . Consequently  $\log(|1 + F|^2) = \log((1 - |F|)^2) \sim -2|F|$ . A modulation instability at a side mode resonance (typically the first) is almost guaranteed. There is a modulation instability for any non-zero proportional gain if the bandpass filter is not present. Only the band pass filter provides slight damping and hence a finite proportional gain range for stability.

Figure 7 provides the predicted locations of the poles for a proportionally controlled oscillator with a single term all-pass loop filter. The example is contrived but it illustrates well the general behaviour of the pole displacements responsible for modulational instability.

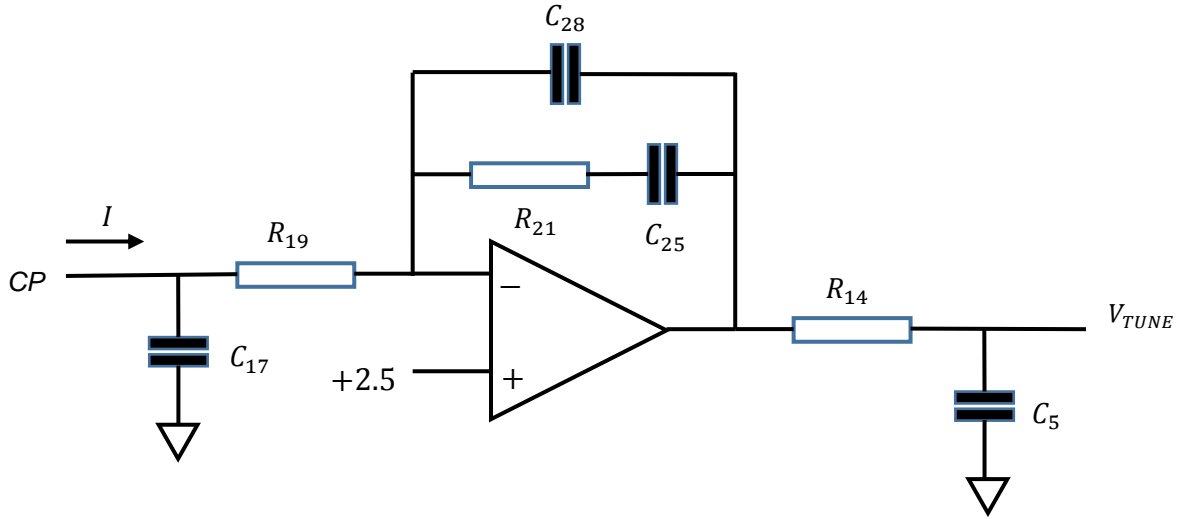


Figure 8 Active loop filter as used in a phase locked loop evaluation board.

$R_{19}$	33 k $\Omega$	$C_{17}$	470 pF	$R_{19}$	22 k $\Omega$	$C_{17}$	2.2 nF
$R_{21}$	33 k $\Omega$	$C_{25}$	47 nF	$R_{21}$	22 k $\Omega$	$C_{25}$	220 nF
$R_{14}$	1.8 k $\Omega$	$C_{28}$	1 nF	$R_{14}$	2.2 k $\Omega$	$C_{28}$	3.3 nF
		$C_5$	4.7 nF			$C_5$	4.7 nF
$I_{CP} = 2.5$ mA		$K_{VCO} = 4$ kHz/V		$I_{CP} = 2.5$ mA		$K_{VCO} = 4$ kHz/V	
$\tau_R = 80$ ns		$\tau_D = 25$ $\mu$ s (5 km)		$\tau_R = 80$ ns		$\tau_D = 25$ $\mu$ s (5 km)	
Table 1 First scenario loop filter component values and system parameters.				Table 2 Second scenario loop filter component values and system parameters.			

Figure 8 illustrates the active filter as used in a phase-locked loop evaluation board. The active filter system function of the is:

$$F(s) = \frac{1}{N} 2\pi K_{VCO} \tau_D \cdot \frac{1}{(1 + sR_{14}C_5)} \cdot \frac{1}{\left(1 + sR_{21} \frac{C_{25}C_{28}}{C_{25} + C_{28}}\right)} \cdot \frac{(1 + sR_{21}C_{25})}{sR_{19}(C_{25} + C_{28})} \cdot \frac{1}{(1 + sR_{19}C_{17})} \cdot \left(\frac{I_{CP}R_{19}}{2\pi}\right)$$

Equation 35

Two examples of component values and other pertinent system parameters are given in Table 1 and Table 2. The component values listed were provided by filter design software with a charge pump current setting of  $I_{CP} = 2.5 \text{ mA}$  and a static voltage controlled oscillator gain setting of  $\kappa_{VCO} = 4 \text{ kHz/V}$  as measured experimentally. The optoelectronic oscillator operated at 10 GHz. The system reference was provided by a 100 MHz RF source. Consequently, the PLL used a  $N = 100$  frequency divider which has the effect of reducing the loop gain by the same factor.

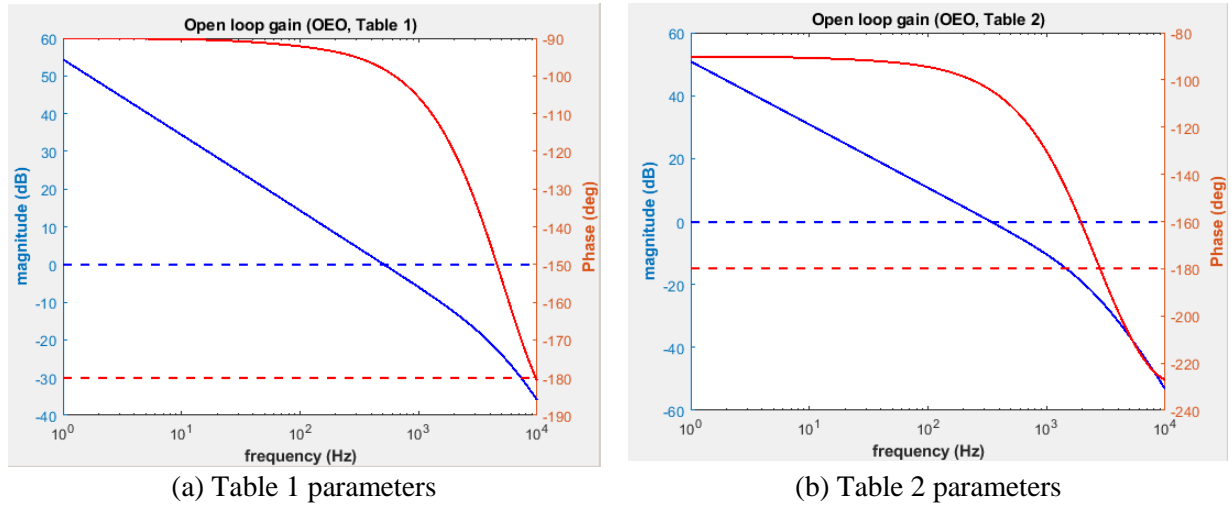


Figure 9 Open loop Bode plots for a PLL-OEO

The component values for both scenarios provided a stable PLL-VCO with substantial phase and gain margins  $\sim 80^\circ$  &  $25 \text{ dB}$ . Figure 9 provides a Bode plot for the PLL-OEO for the two scenarios over a range of offset frequencies up to 10 kHz which superficially indicates stable operation with similar phase and gain margins until one inspects a small neighborhood of the first side-mode resonance at  $\sim 40 \text{ kHz}$  shown in Figure 10 where the phase lag passes through  $-180^\circ$ . For the first scenario parameters the loop gain exceeds unity by up to  $\sim 10 \text{ dB}$  ensuring instability. The second scenario parameters reduce the loop gain at the first side-mode resonance below  $\sim -9 \text{ dB}$  suppressing the instability.

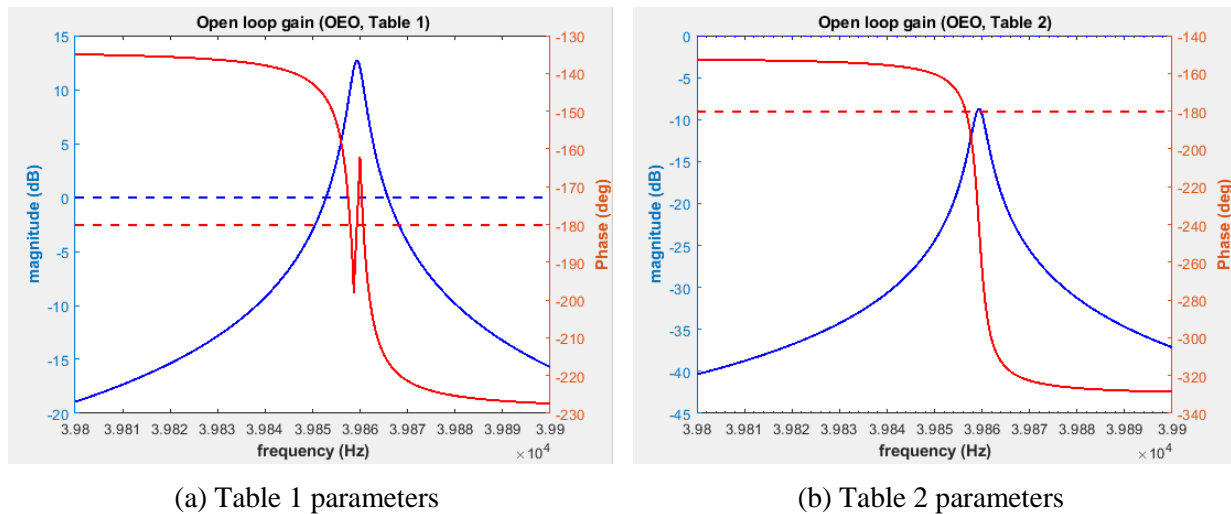


Figure 10 Open loop Bode plots for a PLL-OEO about the first side-mode resonance

The respective predicted outer pole locations of the complete system are illustrated by Figure 11 and Figure 12. For the first scenario modulation instability is observed experimentally for a charge pump current of

800  $\mu A$  or greater. For the second scenario modulation instability is not observed experimentally for charge pump current up to 2.5 mA.

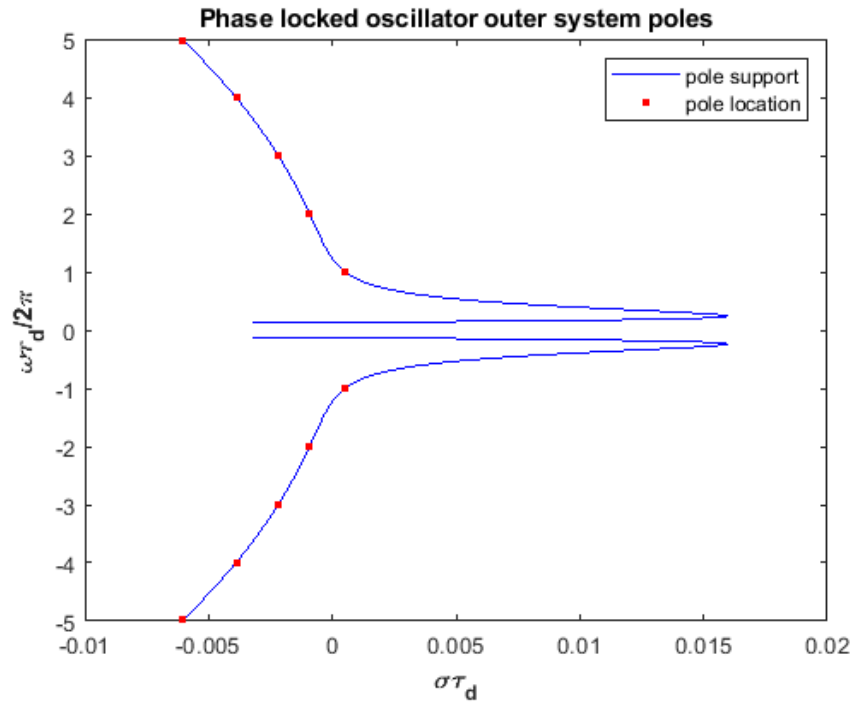


Figure 11 Phase locked oscillator outer system pole locations first scenario. Modulational instability arises due to the small positive real part of the poles associated to the first adjacent side modes.

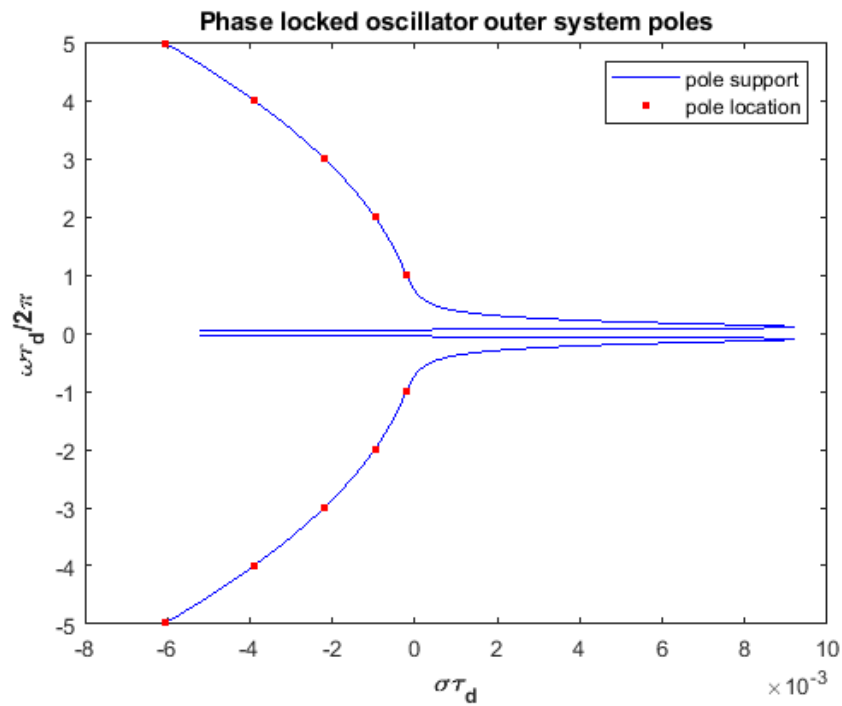


Figure 12 Phase locked oscillator outer system pole locations second scenario. All poles locations have a negative real part albeit slight. Modulational instability is suppressed.

The loop-filter design freedom that is required to achieve performance objectives other than stability such as an engineered phase noise spectrum is seriously curtailed by modulation instability. The restoration of design freedom requires methods of suppressing the spurious resonances that do not re-introduce system reference phase noise. The possibilities include self-injection / self-phase locking, which involve more than one loop, and/or low-noise methods of reducing RF filter bandwidth, which is a challenge.

### VIII. Experimental demonstration

Off the shelf components are used to demonstrate the phase locking of a single loop optoelectronic oscillator. Figure 13 shows a schematic diagram of the experimental arrangement.

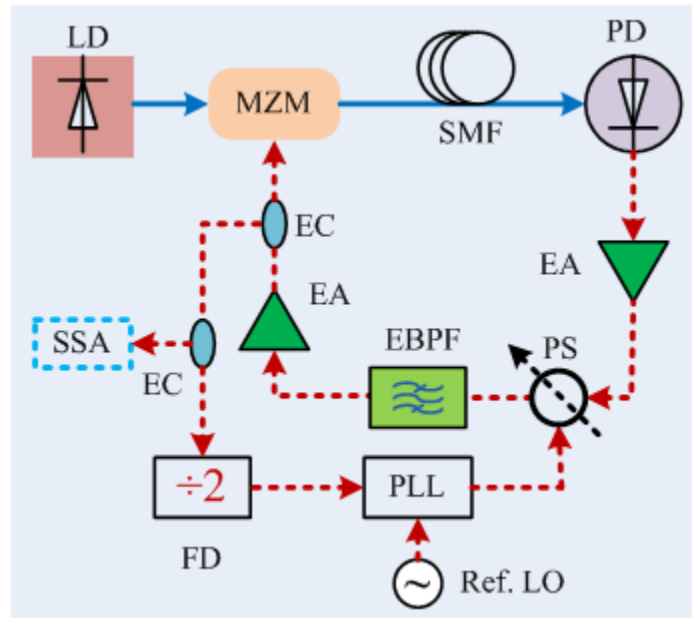


Figure 13 Schematic diagram of the experimental setup for phase locking; PLL, Phase lock loop; FD, Frequency divider; SSA, Signal source analyzer; Ref. LO, Reference local oscillator.

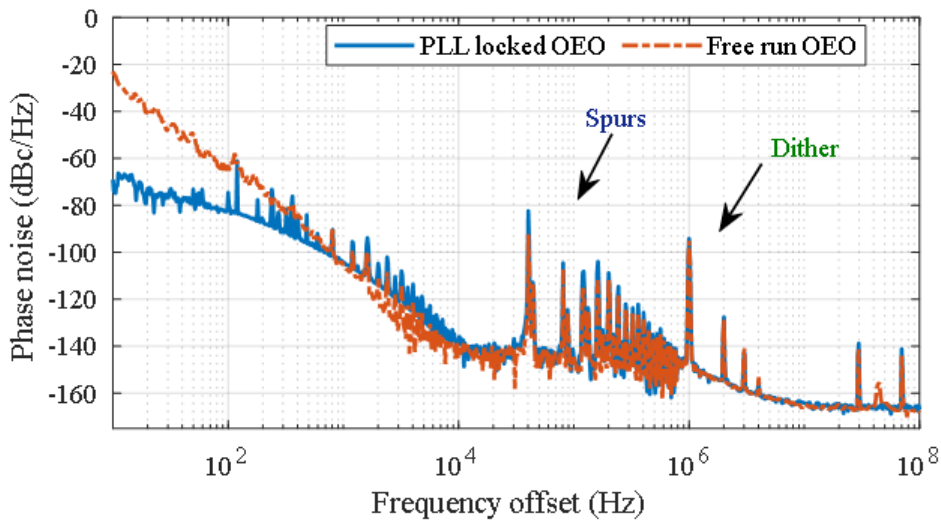


Figure 14 Measured phase noise of the OEO. 100 correlations is used for the measurement.

Analog Devices HMC703 is used as the PLL in this experiment. A Keysight N5166B CXG RF Vector signal generator is used to provide a 100 MHz carrier with power of 6 dBm as reference input. The OEO operates at 10 GHz which is above the 8GHz input frequency limit of the HMC703 is 8 GHz, consequently a  $\div 2$  frequency divider is used before the PLL to bring the signal frequency into the operating range of the PLL. A Keysight signal source analyzer (SSA) E5052B is used to measure the phase noise spectrum of the generated OEO. Figure 14 shows the measured phase noise of the OEO without (Free run OEO) and with PLL locking (PLL locked OEO). 100 correlations is used for the measurement. A phase noise of -141 dBc/Hz @ 10 kHz offset is attained for a carrier frequency of 10.045 GHz. With the increase in correlation to 1000, the phase noise of the OEO improved to -145 dBc/Hz @ 10 kHz offset, however the measurement time thereby becomes prolonged. The spurs at 1 MHz and harmonics are caused by the laser frequency dither is applied to mitigate phase noise due to double Rayleigh scattering (DRS) [19]. The phase locked spectrum also shows that the bandwidth of the active loop filter needs to be reduced further to align the locked OEO with the free run OEO outside the loop filter bandwidth. Nevertheless, a detail method of phase locking of an OEO is demonstrated here. If required the frequency drift compensation can be enlarged further using the method presented in [20].

## IX. Conclusion

This paper reports findings of a study of an optoelectronic oscillator OEO with large delay under proportional and proportional integral control by a phase-locked loop (PLL). The study is the first to fully account for the OEO delay in responding to a tuning stimulus including the location of all of the countable infinity of poles of the system function. This provides a well characterised basic subsystem from which more complex architectures may be considered to be composed, either as nested control loops or as coupled oscillators. The theoretical considerations are supported by experimental observations. The first observation is reported of an OEO exhibiting a giant phase modulation oscillation that is related to the FM mode regime of a mode-locked laser but without the pulse mode regime. The giant phase modulation is a manifestation of a modulation instability of a PLL-OEO system which is described by the analysis and observed experimentally. Nevertheless, the analysis and experimental observations, including a prototype 10 GHz PLL-OEO phase noise spectral density achieving  $-80$  dBc/Hz at at 10 Hz and  $-145$  dBc/Hz at 10 kHz demonstrate that stable phase lock operation and near optimum phase noise performance is achievable provided full account of the multimode operation of the basic oscillator is taken in the phase lock analysis.

## Acknowledgements

Mehedi Hasan and Trevor J. Hall are indebted to Nanowave Technologies Inc. for providing access to their state-of-the-art laboratory to conduct the experimental result presented here. Mehedi Hasan is grateful to the Natural Sciences and Engineering Research Council of Canada (NSERC) for their support through the Vanier Canada Graduate Scholarship program. Trevor J. Hall is grateful to the University of Ottawa for their support of a University Research Chair.

## References:

- [1] T. Hao , J. Tang, D. Domenech , W. Li , N. Zhu , J. Capmany , M. Li, ‘ Toward monolithic integration of OEOs: from systems to chips’, *JLT.*, 36(19), 4565- 4582 (2018).
- [2] X. S. Yao , L. Maleki, ‘Optoelectronic oscillator for photonic systems’, *IEEE J. Quant. Electron.*, **32**(7), 1141–1149, (1996)
- [3] L. Zhang, A. K. Poddar, U. L. Rohde, A. S. Daryoush, ‘ Comparison of optical self-phase locked loop techniques for frequency stabilization of oscillators’, *IEEE Photonics Journal*, **6**(5), 7903015, (2014)
- [4] Y. Zhang, D. Hou, J. Zhao, ‘Long-term frequency stabilization of an optoelectronic oscillator using phase-locked loop’, *J. Lightwave Techn.*, **32**(13), 2408-2414, (2014).
- [5] A. Bluestone, D. T. Spencer, S. Srinivasan, D. Guerra, J. E. Bowers, L. Theogarajan, ‘An ultra-low phase-noise 20-GHz PLL utilizing an optoelectronic voltage-controlled oscillator’, *IEEE Trans. MTT*, **63**(3), 1046-1052, (2015).

- [6] Z. Zhenghua, Y. Chun, C. Zhewei, C. Yuhua, L. Xianghua, 'An Ultra-Low Phase Noise and Highly Stable Optoelectronic Oscillator Utilizing IL-PLL', *IEEE Photonics Technology Letters*, **28**(4), 516-519, 2016.
- [7] R. Fu, X. Jin, Y. Zhu, X. Jin, X. Yu, S. Zheng, H. Chi, X. Zhang, 'Frequency stability optimization of an OEO using phase-locked-loop and self-injection-locking', *Optics Communications* **386**, 27–30, (2017).
- [8] A. Banerjee, L. A. Dantas de Britto, G. M. Pacheco, 'A theoretical and experimental study of injection-pulling for IL-PLL optoelectronic oscillator under RF signal injection', *Optik*, **203**, 164059, (2020).
- [9] R. Adler, "A study of locking phenomena in oscillators," *Proc. IRE*, **34**(6), 351–357, (1946).
- [10] L. J. Paciorek, 'Injection locking of oscillators', *Proc. IEEE*, **53**(11), 1723-1727, (1965).
- [11] L. W. Couch, 'A study of a driven oscillator with FM feedback by use of a phase-locked loop model', *IEEE Trans. Microwave Theory & Techniques*, **MTT-19**(4), 357-366, (1971).
- [12] D. Brunner, B. Penkovsky, B. A. Marquez, M. Jacquot, I. Fischer, L. Larger, 'Tutorial: Photonic neural networks in delay systems', *J. Appl. Physics*, **124**, 152004 (1-15), (2018).
- [13] Y. K. Chembo, 'Machine learning based on reservoir computing with time-delayed optoelectronic and photonic systems', *Chaos*, **30**, 013111 (2020).
- [14] R. Sipahi, S.-I. Niculescu, C. T. Abdallah, W. Michiels, K. Gu, 'Stability and stabilization of systems with time delay', *IEEE Control Systems Magazine*, 38-65, (2011).
- [15] D. B. Leeson, 'Oscillator Phase Noise: A 50-Year Review', *IEEE Trans. Ultrasonics, Ferroelectrics & Frequency Control*, **63**(8), 1208-1225, (2016)
- [16] R. Coreless, G. Gonnet, D. Hare, D. Jeffrey, D. Knuth, 'On the Lambert w function', *Advances in Computational Mathematics.*, **5**, 329-359, (1996).
- [17] S. Yanchuk, G. Giacomelli, 'Spatio-temporal phenomena in complex systems with time delays'. *J. Phys. A: Math. Theor.* **50**, 103001, (2017).
- [18] S. Longhi, P. Laporta, 'Floquet theory of intracavity laser frequency modulation', *Phys. Rev. A*, **60**(5), 4016-4028, (1999).
- [19] O. Lelièvre, V. Crozatier, P. Berger, G. Baili, O. Llopis, D. Dolfi, P. Nouchi, F. Goldfarb, F. Bretenaker, L. Morvan, G. Pillet, 'A model for designing ultralow noise single- and dual-loop 10-GHz optoelectronic oscillators', *Journal of Lightwave Technology*, **35**(20), 4366-4374, (2017).
- [20] J. Dai, Z. Zhao, Y. Zeng, A. Liu, T. Zheng, F. Yin, Y. Zhou, Y. Liu, and K. Xu, "Stabilized optoelectronic oscillator with enlarged frequency-drift compensation range," *IEEE Photonics Technology Letters*, vol. 30, no. 14, pp. 1289-1292, 15 July 2018.